

# Soot Formation in Shock-Tube Pyrolysis of Toluene, Toluene–Methanol, Toluene–Ethanol, and Toluene–Oxygen Mixtures

A. ALEXIOU and A. WILLIAMS\*

*Department of Fuel and Energy, Leeds University, Leeds LS2 9JT, U.K.*

Soot formation during the pyrolysis of argon diluted mixtures of toluene and binary mixtures of toluene–methanol and toluene–ethanol, and during the oxidation of toluene has been studied in a reflected shock tube. Soot induction times and rates of soot formation were measured at 632.8 and 1152.0 nm by a laser beam attenuation method and these showed an Arrhenius dependence on shock temperature. Soot yields and soot amounts were also measured. The soot yield and amount were found to decrease with the addition of methanol and ethanol to toluene, with more pronounced effects for the methanol addition. The addition of oxygen to toluene strongly suppressed soot with a shift of the soot yield to lower temperatures. This last effect was not found during alcohol addition to the toluene and therefore an alternative route to the soot formation at lower temperatures is suggested. A kinetic model was used to interpret the experimental trends and reasonably reproduced the experimental observations. However, the lack of good quantitative agreement emphasised the urgent need in establishing reliable kinetic data and reaction pathways on the oxidation of the benzyl radical and PAH species.

## INTRODUCTION

Hydrocarbon fuels produce soot under pyrolytic or rich combustion conditions and this is a function of the fuel–oxygen ratio, fuel type, and combustion temperature. The mechanism is generally assumed to involve the decomposition of the initial parent hydrocarbon fuel to give ethyne, the formation of benzene from ethyne and further reaction to form increasingly larger polyaromatic hydrocarbon (PAH) molecules. Once sufficiently large PAH species are formed, dimerization results in particle inception with continued growth by ethyne addition. Shock tube studies of soot formation show a near Gaussian shape distribution of the soot yield curve as a function of temperature, and which is frequently termed “bell shape”. Its shape is due to the slow soot forming reactions at low temperature, whereas at higher temperatures the reverse rates become controlling [1]. When oxygen is present, either as molecular oxygen or from the presence of an oxygen atom containing molecule such as an alcohol, soot precursors and/or soot particles may be oxidised by  $O_2$ ,  $O$ , or  $OH$ . The addition of small amounts of oxygen to hydrocar-

bon pyrolysis results in a shift of the soot yield to lower temperatures; this has been attributed to the reactions of molecular oxygen which alter the initial route to soot as well as involving the oxidative removal of PAH [1–3].

The use of alcohols as an alternative fuel is of considerable practical significance because they are easily obtained from renewable resources. They may be used as a blend with petroleum fuels for internal combustion engines. As a blending agent, alcohols are also of considerable significance as one of the simplest oxygen-containing fuel molecules with the ability to suppress soot in flames [4]. Surprisingly, there has been little previous shock tube work on gas phase combustion of alcohol related to soot formation, and only benzene–methanol, benzene–ethanol [5], and some preliminary results on toluene–methanol [6] have been studied. In the present work the effect of the addition of the alcohols, methanol and ethanol, on an aromatic hydrocarbon, toluene, is further evaluated and a comparison is made with the addition of an equivalent amount of molecular oxygen to toluene. The delay time which is required for soot to form, the rates of soot formation, the soot yield and soot amount were measured for argon diluted mixtures of toluene–methanol, toluene–ethanol and toluene–oxygen. A computer model was used

\*Corresponding author.

to interpret the experimental observations and to further understand the behaviour of such mixtures. The kinetic model describes the initial fuel pyrolysis and oxidation, PAH growth and soot particle inception and growth.

### EXPERIMENTAL METHOD

The experiments were formed using a reflected shock tube [7]. A stainless steel shock tube with 73.7 mm in internal diameter and with driver and test sections of 2.44 and 3.35 m long, respectively, was used. The shock waves were initiated using a hand operated plunger to rupture the diaphragm which was made of Melinex (35  $\mu\text{m}$ ). A flush-fitting Kistler 603 B quartz pressure transducer was mounted in the center of the end plate of the test section which served as a trigger in shock speed determination and laser attenuation studies. Four observation windows, of 5 mm diameter each one, were located at 12.5 mm from the end plate at 90° to each other and allowed measurements to be taken. Incident shock velocity measurements were obtained using five piezoelectric detectors. Reflected shock conditions were calculated using the method given by Gardiner et al. [8]. The test gas mixtures were prepared manometrically. The stated purities of the gases were as follows: toluene, 99.96% (Analar BDH sulphur free); methanol, 99.8% (Analar BDH); ethanol, 99.9%; oxygen, 99.96% (BOC); argon, 99.995% (BOC); helium, 99.99% (BOC). Toluene, methanol and ethanol were further purified by repeated freezing and evacuation. The experimental conditions are summarised in Table 1. The soot conversion was determined by measuring the attenuation of the beams from a 15 mW He-Ne Spectra-Physics laser at 632.8 nm and at 1152.0 nm from a 3-mW He-Ne gas laser. The soot yield,  $Y$ , was calculated using Graham's model [9]:

$$Y = \frac{[C]_{\text{soot}}}{[C]_{\text{total}}} = \frac{N_{AV} \rho \lambda}{72 \pi E_{(m)} l [C]_{\text{total}}} \ln \frac{I_0}{I}, \quad (1)$$

where

$[C]_{\text{soot}}$  is the concentration of carbon atoms in the soot particles formed,  
 $[C]_{\text{total}}$  is the initial concentration of carbon atoms in the fuel,

$N_{AV}$  is the Avogadro number,  
 $\rho$  is the density,  
 $\lambda$  is the wavelength,  
 $l$  is the length of the optical path, which in the shock tube in this study is equal 0.0737 m,  
 $I_0$  is the intensity of incident light,  
 $I$  is the intensity of transmitted light.  
 $E_{(m)}$  is a function of the complex refractive index,  $m = n - ik$ , and is equal to:

$$E_{(m)} = -I_m \left[ \frac{m^2 - 1}{m^2 + 2} \right] = \frac{6nk}{(n^2 - k^2 + 2)^2 + 4n^2k^2}, \quad (2)$$

where

$I_m$  [ ] is the imaginary part of [ ],  $n$  is the real part of the complex refractive index, and  $k$  is the imaginary part of the complex refractive index.

The term "soot yield" which is defined above, and which is the fractional conversion of the carbon atoms in a hydrocarbon fuel to soot, and "soot amount" which is the absolute amount of carbon atoms ( $\text{cm}^{-3}$ ) in the soot produced were both used as appropriate practical measurements of soot formation. These measurements provide essentially identical information, however, it is necessary to use both definitions when binary hydrocarbon mixtures are used to give a better indication of sooting tendencies [10]. The values of  $E_{(m)}$  which were used in the interpretation of the laser signals are those of Charalampopoulos and Chang [12, 13] which are equal to  $E_{(m)} = 0.253$  and  $E_{(m)} = 0.22$  for the visible (632.8 nm) and infrared (1152.0 nm) wavelengths respectively. Further discussion about their choice is given later.

### EXPERIMENTAL RESULTS

#### Soot Induction Time

During the course of the soot formation experiments, a soot induction period,  $\tau_{\text{soot}}$ , defined as the time interval between the reflected pressure signal and the onset of attenuation (1%

TABLE I  
Experimental Conditions Behind Reflected Shock Waves

Mixt. mol % in Ar	T(K)	P(Bar)	Carbon Atoms cm <sup>-3</sup>
0.5 C <sub>7</sub> H <sub>8</sub>	1826–2233	1.95–2.62	2.705–2.97 10 <sup>17</sup>
1.0 C <sub>7</sub> H <sub>8</sub>	1668–2424	1.87–3.29	5.68–6.90 10 <sup>17</sup>
1.5 C <sub>7</sub> H <sub>8</sub>	1566–2345	1.93–3.5	0.938–1.15 10 <sup>18</sup>
1.0 C <sub>7</sub> H <sub>8</sub> + 0.3 CH <sub>3</sub> OH	1652–2391	1.87–3.3	5.98–7.29 10 <sup>17</sup>
1.0 C <sub>7</sub> H <sub>8</sub> + 0.5 CH <sub>3</sub> OH	1625–2426	1.84–3.41	6.147–7.63 10 <sup>17</sup>
1.0 C <sub>7</sub> H <sub>8</sub> + 1.0 CH <sub>3</sub> OH	1655–2087	1.9–2.79	6.648–7.74 10 <sup>17</sup>
1.0 C <sub>7</sub> H <sub>8</sub> + 2.0 CH <sub>3</sub> OH	1664–2365	2.06–3.55	8.06–9.779 10 <sup>17</sup>
1.5 C <sub>7</sub> H <sub>8</sub> + 2.0 CH <sub>3</sub> OH	1548–2075	1.99–3.21	1.16–1.4 10 <sup>18</sup>
1.0 C <sub>7</sub> H <sub>8</sub> + 1.0 C <sub>2</sub> H <sub>5</sub> OH	1610–2275	1.95–3.34	7.95–9.56 10 <sup>18</sup>
1.0 C <sub>7</sub> H <sub>8</sub> + 2.0 C <sub>2</sub> H <sub>5</sub> OH	1546–2223	2.01–3.56	1.03–1.27 10 <sup>18</sup>
1.0 C <sub>7</sub> H <sub>8</sub> + 3.0 C <sub>2</sub> H <sub>5</sub> OH	1565–2085	2.24–3.55	1.34–1.6 10 <sup>18</sup>
1.5 C <sub>7</sub> H <sub>8</sub> + 2.5 C <sub>2</sub> H <sub>5</sub> OH	1480–2108	2.12–3.77	1.60–2.0 10 <sup>18</sup>
1.0 C <sub>7</sub> H <sub>8</sub> + 0.5 O <sub>2</sub>	1581–2258	1.73–2.99	5.56–6.73 10 <sup>17</sup>
1.0 C <sub>7</sub> H <sub>8</sub> + 1.0 O <sub>2</sub>	1517–2110	1.63–2.72	5.44–6.65 10 <sup>17</sup>
1.5 C <sub>7</sub> H <sub>8</sub> + 1.5 O <sub>2</sub>	1473–2213	1.7–3.26	0.87–1.13 10 <sup>18</sup>
1.5 C <sub>7</sub> H <sub>8</sub> + 2.5 O <sub>2</sub>	1447–2064	1.66–2.96	0.87–1.09 10 <sup>18</sup>
1.0 C <sub>7</sub> H <sub>8</sub> (1152 nm)	1565–2406	1.69–3.27	5.47–6.89 10 <sup>17</sup>
1.5 C <sub>7</sub> H <sub>8</sub> (1152 nm)	1612–2317	1.94–3.44	0.91–1.13 10 <sup>18</sup>
1.5 C <sub>7</sub> H <sub>8</sub> + 2.5 C <sub>2</sub> H <sub>5</sub> OH (1152 nm)	1447–2064	1.67–2.96	0.87–1.09 10 <sup>18</sup>

signal rise) ranging from approximately 20–2100  $\mu$ s was observed before any absorption occurred. Correlation equations for the delay time were obtained for the pyrolysis of toluene, toluene-methanol, toluene-ethanol, and toluene-oxygen mixtures diluted in argon, within the range of experimental conditions given in Table 1 and these are as follows:

$\tau_{\text{soot}}(632.8 \text{ nm})$

$$= 8.42 \times 10^{-12} \exp\left(\frac{181}{RT}\right) [\text{C}_7\text{H}_8]^{-1.57},$$

( $R' = 84.4\%$ ), (3)

$\tau_{\text{soot}}(1152.0 \text{ nm})$

$$= 1.25 \times 10^{-9} \exp\left(\frac{157}{RT}\right) [\text{C}_7\text{H}_8]^{-0.766},$$

( $R' = 95.6\%$ ), (4)

$\tau_{\text{soot}}(632.8 \text{ nm})$

$$= 1.25 \times 10^{-11} \exp\left(\frac{164}{RT}\right) \times [\text{C}_7\text{H}_8]^{-2.21} [\text{CH}_3\text{OH}]^{0.16},$$

( $R' = 91.8\%$ ), (5)

$\tau_{\text{soot}}(632.8 \text{ nm})$

$$= 1.2 \times 10^{-14} \exp\left(\frac{192}{RT}\right) \times [\text{C}_7\text{H}_8]^{4.48} [\text{C}_2\text{H}_5\text{OH}]^{0.825},$$

( $R' = 84.6\%$ ), (6)

$\tau_{\text{soot}}(632.8 \text{ nm})$

$$= 1.03 \times 10^{-11} \exp\left(\frac{196}{RT}\right) \times [\text{C}_7\text{H}_8]^{-1.24} [\text{O}_2]^{0.364},$$

( $R' = 96.0\%$ ), (7)

where  $\tau_{\text{soot}}$  is the induction time for soot appearance (s),  $T$  is the reflected shock temperature (K),  $R$  is the gas constant (kJ mol<sup>-1</sup> K<sup>-1</sup>), while the initial post-shock concentrations of the fuel mixtures are in mol m<sup>-3</sup>. The square of the correlation coefficient  $R'$ , obtained during the statistical analysis is also given. These empirical global expressions are useful in representing a large number of complex reactions in a condensed way and give some indication of the influence of the main parameters. The measured induction times for soot appearance showed an Arrhenius dependence on the reflected shock temperature ( $T_5$ ). The minus exponent in the toluene dependency indicates

that the soot forms earlier as the partial pressure of toluene is increased.

The empirical expressions also shown that the effect of alcohol addition to toluene is to reduce the induction time compared to toluene alone, with a very pronounced effect for ethanol addition. During toluene oxidation with molecular oxygen the induction time for soot formation is increased. Also the results obtained using the infrared laser (1152.0 nm) showed longer induction times compared to the visible (632.8 nm). This essentially arises because the use of an infrared laser at 1152.0 nm only determines soot particles and extremely large molecules (molecular weight  $\gg$  500), whereas at 632.8 nm there is additional absorption by soot precursors, i.e., PAH molecules [14].

#### Rates of Soot Formation

The maximum rate of soot formation was determined from the maximum slope value of the soot formation curve; it varied with temperature and concentration of the hydrocarbon or oxygen used. Correlation equations for the rate of soot formation for toluene, toluene-methanol, toluene-ethanol, and toluene-oxygen mixtures, diluted in argon, were determined within the range of experimental conditions given in Table 1 and are given by the following expressions:

$$R_{\text{soot}}(632.8 \text{ nm}) = 6.5 \times 10^6 \exp\left(\frac{-85}{RT}\right) [\text{C}_7\text{H}_8]^{1.32} [\text{Ar}]^{0.194} \quad (R' = 93.1\%), \quad (8)$$

$$R_{\text{soot}}(1152.0 \text{ nm}) = 2.42 \times 10^6 \exp\left(\frac{-91}{RT}\right) [\text{C}_7\text{H}_8]^{1.02} \quad (R' = 94.6\%), \quad (9)$$

$$R_{\text{soot}}(632.8 \text{ nm}) = 5.9 \times 10^6 \exp\left(\frac{-102}{RT}\right) \times [\text{C}_7\text{H}_8]^{1.37} [\text{CH}_3\text{OH}]^{-0.4} \quad (R' = 79.0\%), \quad (10)$$

$$R_{\text{soot}}(632.8 \text{ nm}) = 1.6 \times 10^{10} \exp\left(\frac{-197}{RT}\right) \times [\text{C}_7\text{H}_8]^{2.41} [\text{C}_2\text{H}_5\text{OH}]^{-0.954} \quad (R' = 83.9\%), \quad (11)$$

$$R_{\text{soot}}(632.8 \text{ nm}) = 4.4 \times 10^7 \exp\left(\frac{-128}{RT}\right) \times [\text{C}_7\text{H}_8]^{2.67} [\text{O}_2]^{-1.27} \quad (R' = 80.1\%), \quad (12)$$

where  $R_{\text{soot}}$  is the rate of soot formation in  $\text{mol m}^{-3} \text{s}^{-1}$ . The measured rates of soot formation showed also an Arrhenius dependence on the reflected shock temperature ( $T_5$ ). The positive exponent in the toluene dependency indicates that an increase in partial pressure of toluene increases the soot formation rate. The argon dependency was very small and was only determined for Eq. 8.

From these equations it can be shown that ethanol addition to toluene increased the rate of soot formation whereas methanol and oxygen addition to toluene reduced the rate of soot formation. A reduction of the rate of soot formation was also observed when a comparison between visible and infrared modes of attenuation is made as shown by Eqs. 8 and 9, this arising for reasons set out earlier since the infrared results recorded only the formation and growth of the soot particle without any significant interference by PAH absorption. However, the use of the 632.8 nm laser is convenient because it gives an indication of all soot forming activities as well as a mean of comparison with earlier work.

However, the toluene-methanol, toluene-ethanol, and toluene-oxygen expressions, though adequately describing the range of experimental conditions investigated, do not hold for the condition where no toluene is present. The following expression takes this limitation into consideration:

$$R_{\text{soot}} = F(6.5 \times 10^6) [\text{TotalHydrocarbon}]^{1.32} \times [\text{Ar}]^{0.194} \exp\left(\frac{-85}{RT}\right), \quad (13)$$

where  $F$  is an arbitrary factor depending on the toluene-methanol, toluene-ethanol, and toluene-oxygen ratio. For the mixtures investigated at 1800 K the values of  $F$  are shown in Fig. 1. The effect of *i*-octane and *n*-heptane substitution for toluene are also shown in this figure. A similar trend to that given by the induction time and the rate of soot formation equations can be seen. The value of  $F$  is reduced with increase in the amount of oxygen, methanol or ethanol added to the toluene with more pronounced results for oxygen or methanol addition to toluene. The  $F$  value is sharply reduced when *i*-octane and *n*-heptane were substituted for toluene, which again demonstrates the difference in sooting tendencies between aromatic and aliphatic fuels.

### Soot Yields and Amounts

The soot yield and soot amount results obtained in the toluene pyrolysis using the visible laser (632.8 nm) are shown in Figs. 2 and 3. The soot yields and soot amounts increased with an increase in initial fuel concentration, also with an increase in temperature reaching a maximum and later decreasing giving a Gaussian shape distribution. The distinction in

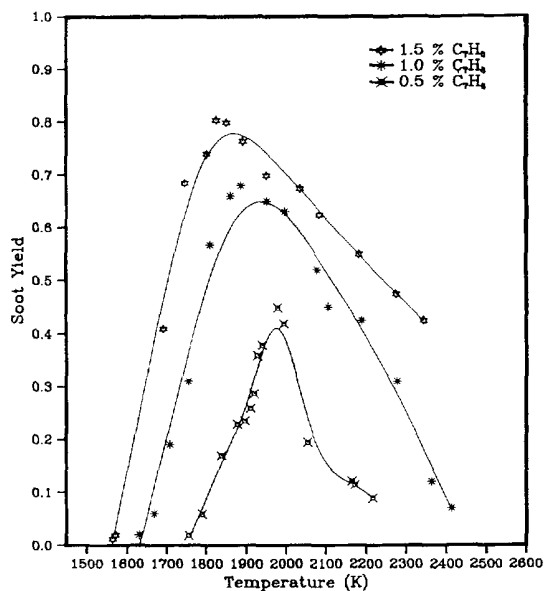


Fig. 2. The soot yield as a function of different toluene concentrations.

the present work between soot particles and gas-phase species is accomplished by using the infrared laser at 1152.0 nm, whereby only soot particles and some extremely large molecules are detected. The difference between the two

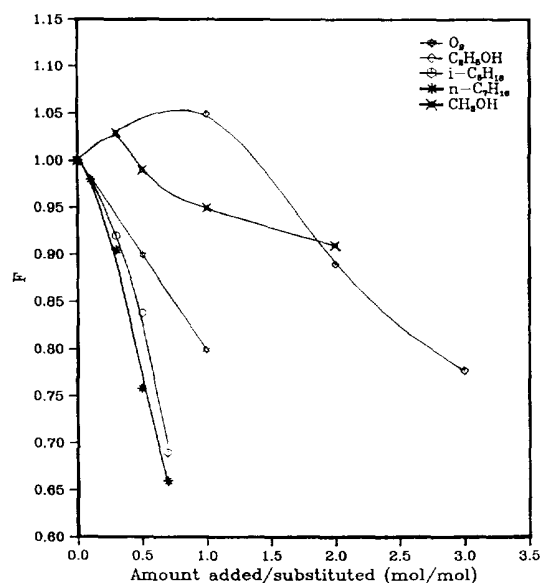


Fig. 1. The  $F$  factor as a function of different fuel concentrations at 1800 K.

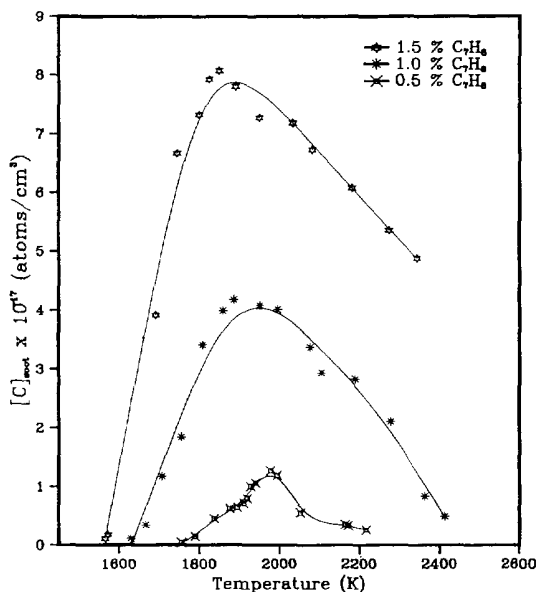


Fig. 3. The soot amount as a function of different toluene concentrations.

laser used is shown in Fig. 4 where visible (632.8 nm) and infrared (1152.0 nm) absorption are compared. The soot yield not only shifted to higher temperatures but a substantial reduction of the soot yield was also obtained.

The effect of methanol and ethanol addition to the toluene yield is shown in Figs. 5–8 where the soot yield and soot amount are plotted versus temperature. Both methanol and ethanol suppress soot, although this reduction is only significant when the methanol exceeds more than 50% and the ethanol exceeds 66.6% in the total fuel mixture to be pyrolysed. Thus methanol suppresses soot slightly more readily than ethanol. The soot yield in the ethanol case is shifted to higher temperatures (Fig. 6) while the soot amount is increased (Fig. 8) indicating a synergistic effect.

Oxygen addition to the toluene not only suppresses soot but shifts the soot yield to lower temperatures as is shown in Fig. 9.

A comparison of the results of alcohol addition to toluene and those obtained during oxidation of toluene is of interest. The results obtained during the oxidation of toluene revealed a strong suppression of soot formation

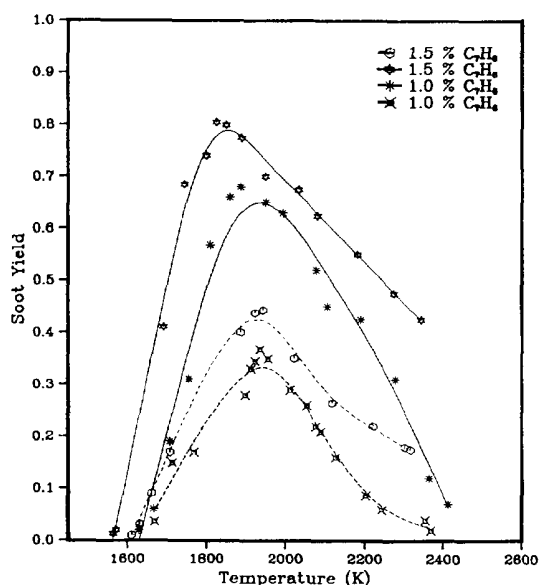


Fig. 4. A comparison of the soot yield in toluene pyrolysis between two wavelengths; 632.8 and 1152.0 nm (dotted lines).

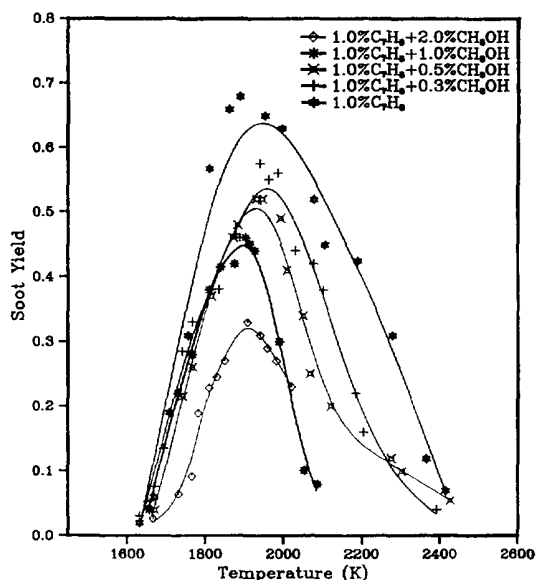


Fig. 5. Soot yield obtained during pyrolysis of toluene/methanol mixtures.

and a shift of the soot yield to lower temperatures. This last effect not only was absent during alcohol addition but showed a small opposite trend during the ethanol addition to the toluene.

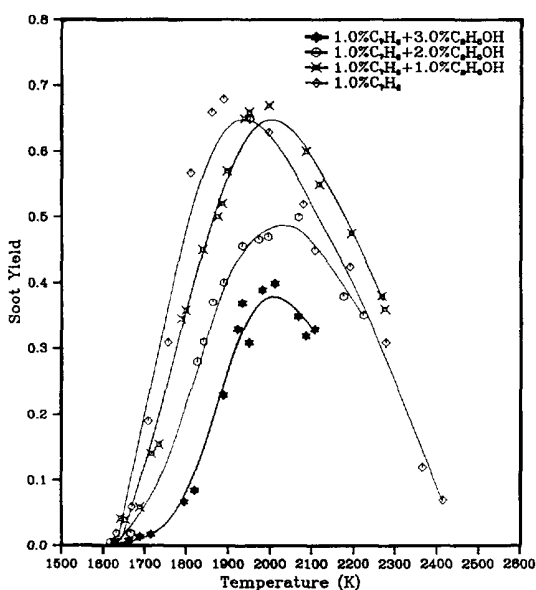


Fig. 6. Soot yield obtained during pyrolysis of toluene/ethanol mixtures.

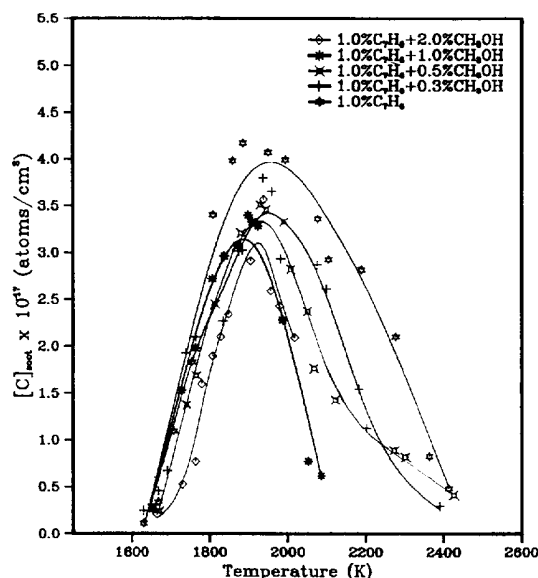


Fig. 7. Soot amount obtained during pyrolysis of toluene/methanol mixtures.

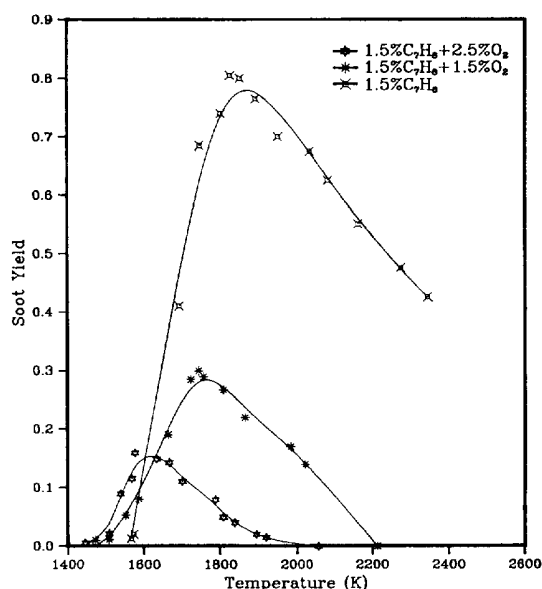


Fig. 9. Soot yield obtained during oxidation of toluene.

## DISCUSSION

### Accuracy of the Measurement Technique

Since the experimentally determined soot yield is a function of the complex refractive index an accurate value is necessarily in literature however, many values of the complex refractive

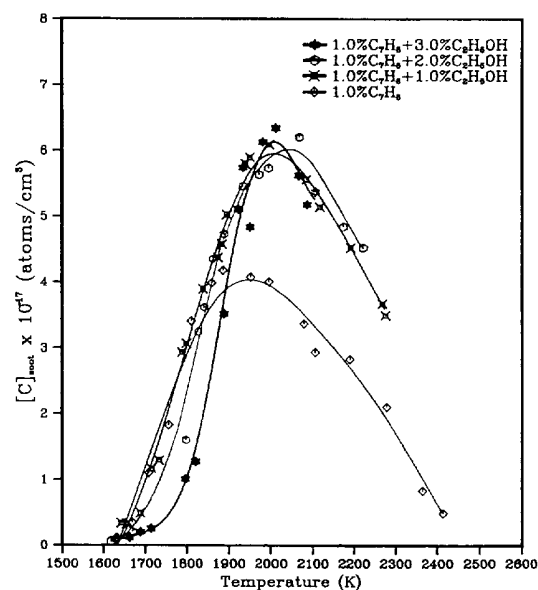


Fig. 8. Soot amount obtained during pyrolysis of toluene/ethanol mixtures.

index of soot have been reported using different techniques, and indeed the mass growth rate of soot may differ by 100% or more when different refractive indices are employed in the data analysis [11]. Previous values of the refractive index of soot have been obtained from studies that may be divided into two categories; those which employed measurement under flame conditions and those made on soot extracted from flames. The difficulty with the latter is that the particle morphology and temperature are not representative of the soot particles under flame conditions [12, 13]. The complex refractive indices that have been most extensively used are those of Dalzell and Sarofim [15] with  $E_{(m)} = 0.135$  at 632.8 nm and of Lee and Tien [16], where  $E_{(m)} = 0.174$  at 632.8 nm. The former used an ex-situ technique where soot particles were collected and compressed into pellets. The latter examined experimentally and theoretically the dependence of the soot index of refraction on the wavelength by employing the Drude-Lorentz dispersion model. They found no temperature dependence and no fuel dependence of the index. More recently Charalampopoulos and Chang [12, 13] demonstrated that by using light scattering to obtain the particle size distribution and by measuring the extinction and scat-

tering coefficient at the same position in a premixed propane flame the refractive index of soot can be determined by introducing a relation between real and imaginary part of the complex electrical permittivity. Charalampopoulos and Chang [12, 13] showed how the refractive index varies with temperature, chemical composition, height above the burner and wavelength. Attempts to use the values given by Dalzell and Sarofim [15] and by Lee and Tien [16] gave over 100% soot conversion. Therefore we adopted the data obtained by Charalampopoulos and Chang [12, 13], with values of  $E_{(m)} = 0.253$  for the visible (632.0 nm) and  $E_{(m)} = 0.22$  for the infrared (1152.0 nm), which gave reasonable conversion levels.

It is very important to compare our experimental results with other data reported in literature [9, 10, 17–19]. Graham et al. [9] concluded that soot yield from toluene alone passes through a maxima around 1800 K after a reaction time of 2.5 ms. They explain these results on the basis that soot formation involves two different pathways; condensation  $\approx 1800$  K and fragmentation  $> 1800$  K; this conclusion was later supported by Wang et al. [18]. Frenklach et al. [19] reinvestigated soot formation from toluene pyrolysis and concluded that soot yield is not universally constant but it depends on experimental variables such as observation time, total pressure, initial hydrocarbon concentration and the wavelength employed in the measurements. In the present work the maximum soot yield and amount are measured irrespective of the observation time. It was found that the maximum occurs at a reaction time greater than 1 ms, the during toluene pyrolysis the soot yield and amount pass through a maximum at  $\approx 1950$  K. The soot yield and soot amount are also found to be a function of initial fuel concentration, total pressure, the wavelength used for the measurements as well as the value of the complex refractive index used in the interpretation of the signal. In view of all these different factors influencing the soot yield and amount the agreement with previously reported data on soot yields and amounts is regarded as satisfactory. However, it is very difficult to compare the induction time and the rate of soot forma-

tion for toluene pyrolysis and oxidation with other reported data [such as 18] since the experimental conditions are different as is the method for interpretation.

In the case of methanol or ethanol addition to toluene, Frenklach and Yuan [5] found the opposite trend when these two fuels were added to benzene. More specifically, and in contrast to the present work, they found that ethanol addition suppresses soot more readily than methanol addition. This probably arises because Frenklach and Yuan determined soot yields at 1 ms rather than the maximum values used in this paper. However, these results show that the ethanol mixture has a longer induction time than methanol and therefore it seems likely that this results in an elongated overall reaction time for the ethanol–benzene and the soot yield has not reached its maximum value.

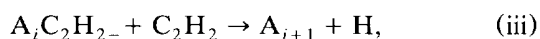
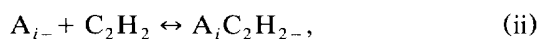
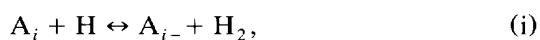
### Kinetic Modelling

*The Soot Model.* The kinetic model of soot formation used during the present work consisted of three stages: (1) initial formation of small PAH species, involving a detailed description of toluene pyrolysis and oxidation as well as oxidative pyrolysis of added methanol and ethanol, some of the key reactions are shown in Table 2, (2) growth of the PAH, and (3) particle inception and growth of the soot particle.

In the first part of the model, both  $C_6H_6$  and  $C_6H_5$  are treated as important intermediate precursors to soot. With aromatic fuels these precursors are already present but with nonaromatic fuels they have to be formed. This begins with  $C_2H_3$  addition to  $C_2H_2$  forming  $C_4H_4$  (R6). At high temperatures  $C_6H_5$  is formed by  $C_2H_2$  addition to  $n-C_4H_3$  radical which is first formed by H atom abstraction from the  $C_4H_4$  (R7 and R8). At lower temperatures the addition of  $C_2H_2$  to  $C_2H_3$  results in  $n-C_4H_5$  (R9) which upon addition of  $C_2H_2$  produces  $C_6H_6$  (R10) [20]. As an alternative to the above mechanism, Miller and Melius [21] suggested that  $C_6H_6$  is formed by combination of  $C_3H_3$  radicals producing  $C_6H_6$  (R11); both equations are used in our mechanism.



The second part of the model describing PAH growth is that given by Frenklach et al. [10, 20]. Two of the main features of this scheme are the formation of stable PAH molecules by ethyne addition and their reactivation by hydrogen atom abstraction, reactions (i) to (iii).



where  $A_i$  denotes an aromatic molecule containing  $i$  fused aromatic rings,  $A_{i-}$  is an aromatic radical formed by the abstraction of a hydrogen atom from  $A_i$ , and  $A_iC_2H_{2-}$  is a radical formed by the addition of  $C_2H_2$  to  $A_{i-}$ . It is assumed that reaction (i) and (ii) are reversible and reaction (iii) irreversible.

All the large PAH species which are formed in the second stage of the model are assumed to collide giving rise to a nucleus. Different combinations of PAH monomers were assumed to collide and form dimers, the dimers

TABLE 2

Some of the Initial Key Reactions Used in the Present Work:  $k = AT^n \exp(-E/RT)$  (units mol, s, cm<sup>-3</sup>, kJ, K)

$k$	Reaction	$A$	$n$	$E$	Ref.
R1	$C_7H_8 \rightarrow C_7H_7 + H$	$3.9 \times 10^{15}$	0	374	29
R2	$C_7H_8 \rightarrow C_6H_5 + CH_3$	$1.5 \times 10^{15}$	0	394	26
R3	$C_7H_7 \rightarrow C_5H_5 + C_2H_2$	$1.0 \times 10^{15}$	0	146	29
R4	$C_7H_7 \rightarrow C_4H_4 + C_3H_3$	$2.0 \times 10^{15}$	0	349	29
R5	$C_5H_5 \rightarrow C_3H_3 + C_2H_2$	$1.0 \times 10^{14}$	0	71	29
R6	$C_2H_3 + C_2H_2 \rightarrow C_4H_4 + H$	$1.6 \times 10^{13}$	0	104	34
R7	$C_4H_4 + H \rightarrow n - C_4H_3 + H$	$1.5 \times 10^{14}$	0	42.6	36
R8	$n - C_4H_3 + C_2H_2 \rightarrow C_6H_5$	$7.0 \times 10^{14}$	-0.8	26.6	36
R9	$C_2H_3 + C_2H_2 \rightarrow n - C_4H_5$	$1.0 \times 10^{13}$	0	0	10
R10	$n - C_4H_5 + C_2H_2 \rightarrow C_6H_6 + H$	$2.4 \times 10^8$	1.18	15.6	10
R11	$2 \times C_3H_3 \rightarrow C_6H_6$	$3.0 \times 10^{11}$	0	0	37
R12	$CH_3OH \rightarrow CH_3 + OH$	$1.9 \times 10^{16}$	0	384	30
R13	$CH_3OH \rightarrow CH_2OH + H$	$1.5 \times 10^{16}$	0	404	30
R14	$C_2H_5OH \rightarrow CH_3 + CH_2OH$	$2.3 \times 10^{19}$	-0.9	365	30
R15	$C_2H_5OH \rightarrow C_2H_5 + OH$	$4.6 \times 10^{19}$	-0.9	394	30
R16	$C_2H_5OH \rightarrow C_2H_4 + H_2O$	$1.0 \times 10^{14}$	0	320.9	31
R17	$C_2H_5OH + OH \rightarrow C_2H_4OH + H_2O$	$4.52 \times 10^{12}$	0	2.99	30
R18	$C_2H_5OH + H \rightarrow C_2H_4OH + H_2$	$2.64 \times 10^{12}$	0	19.12	30
R19	$C_2H_4OH \rightarrow C_2H_4 + OH$	$3.23 \times 10^{14}$	-0.24	140.8	30
R20	$C_2H_5 + M \rightarrow C_2H_4 + M$	$2.0 \times 10^{15}$	0	30.0	44
R21	$C_2H_4 + H \rightarrow C_2H_3 + H + M$	$6.3 \times 10^{18}$	0	108	44
R22	$C_2H_4 + H \rightarrow C_2H_3 + H_2$	$1.5 \times 10^7$	2.0	6.0	44
R23	$C_2H_3 + M \rightarrow C_2H_2 + H + M$	$7.9 \times 10^{14}$	0	31.5	44
R24	$C_2H_3 + H \rightarrow C_2H_2 + H_2$	$2.0 \times 10^{13}$	0	2.5	44
R25	$C_7H_8 + O_2 \rightarrow C_7H_7 + HO_2$	$1.0 \times 10^{14}$	0	84.1	38
R26	$C_7H_7 + HO_2 \rightarrow C_6H_5CH_2O + O$	$5.0 \times 10^{12}$	0	0	33
R27	$C_7H_7 + O \rightarrow C_6H_5CHO + H$	$4.0 \times 10^{14}$	0	0	33
R28	$C_7H_7 + OH \rightarrow C_6H_5CH_2OH$	$2.0 \times 10^{13}$	0	0	33
R29	$C_6H_5CH_2O \rightarrow C_6H_5CHO + H$	$1.0 \times 10^{10}$	0	0	39
R30	$C_6H_5CH_2OH + OH \rightarrow C_6H_5CH_2O + H_2O$	$5.0 \times 10^{12}$	0	0	33
R31	$C_6H_5CHO \rightarrow C_6H_5CO + H$	$1.0 \times 10^{10}$	0	30.3	40
R32	$C_6H_6 + OH \rightarrow C_6H_5 + H_2O$	$2.1 \times 10^{13}$	0	19.2	41
R33	$C_6H_6 + O_2 \rightarrow C_6H_5 + HO_2$	$6.3 \times 10^{13}$	0	251	43
R34	$C_6H_5 + O_2 \rightarrow C_6H_5O + O$	$1.0 \times 10^{13}$	0	0	1
R35	$C_6H_5O \rightarrow C_5H_5 + CO$	$2.5 \times 10^{11}$	0	184	43
R36	$C_5H_5 + OH \rightarrow C_5H_4OH + H$	$1.0 \times 10^{13}$	0	0	43
R37	$C_5H_4OH \rightarrow C_4H_4 + HCO$	$1.0 \times 10^{15}$	0	0	43
R38	$C_4H_4 + OH \rightarrow C_4H_3 + H_2O$	$1.0 \times 10^7$	2	8.37	21

further colliding with other monomers or dimers forming trimers etc. Such a combination of PAH reactions resulted in particle inception. These reactions are treated as irreversible [20]. Miller [22] found that agglomeration becomes important when the reduced mass of the colliding pair is greater than 400 amu, in the current work a maximum size of 15 rings ( $A_{15} \approx 600$  amu) was formed before any collisions of PAH were assumed to take place. This particular part of the model is essential in particle inception since the process of ethyne addition to the PAH and hydrogen abstraction (reactions i to iii) was found to be very slow in producing the required size of the nucleus. This conclusion is also supported by earlier studies by McKinnon and Howard [23]. A minimum size of the soot nucleus of 1 nm was assumed [24]. The growth of the incipient particle is based on the model described by Harris and Weiner [11] and is given by Eq. 14.

$$\frac{dM}{dt} = kS[C_2H_2]. \quad (14)$$

Here  $M$  is the total soot mass in  $\text{g cm}^{-3}$ ,  $S$  is the surface area  $\text{cm}^2 \text{cm}^{-3}$ , and  $k$  is the rate constant for the reaction which adds ethyne into soot, which is the present work was taken equal to  $5 \times 10^{-3} \text{ g cm}^{-2} \text{ s}^{-1} \text{ atm}^{-1}$  [11]. It was also assumed that the main mass of soot growth is formed by heterogeneous reactions of  $C_2H_2$ . The growth by  $C_4H_2$  and  $C_6H_6$  was tested using equation 14, but was found very small compared to growth by ethyne. The contribution of the larger hydrocarbons was also found to be small. However, it is believed that the dimerization of PAH played an indirect role, in soot growth, by initially supplying the surface area for growth. The larger the molecule taking place in the dimerization process the larger the incipient particle is formed and thus the larger the surface area for subsequent growth by ethyne and PAH.

**Toluene Pyrolysis.** Toluene decomposition involves the reactions R1 and R2 as given in Table 2 [25–29]. The structural form of  $C_7H_7$  is still uncertain, however, further decomposition reactions of  $C_7H_7$  would lead to  $C_2H_2$  formation (R3–R5). There has been consider-

able controversy about the relative rates of these two initiation reaction. Pamidimukkala et al. [25] we used both time-of-flight-mass-spectrometer and laser-schlieren-densitometry over the temperature range of 1550–2200 K, found that methane is one of the major species in toluene dissociation, although ethyne is formed in greater quantities. Rao and Skinner [26] using atomic-resonance-absorption-spectroscopy concluded that reaction R2 increases in importance with temperature and is the dominant one above 1600 K. In contrast to Rao and Skinner [26], Brouwer et al. [27] concluded that reaction R1 is the dominant reaction, provided a faster benzyl decomposition, and this was also supported by others [28, 29]. The computed concentration profiles of some species as a function of time for 1.0 mol %  $C_7H_8$ , at 2000 K, are shown in Fig. 10. The nomenclature used for the aromatic species shown in Fig. 10 is that taken from Ref. 1; thus A7 represents a PAH molecule containing 7 rings.  $C_{\text{nuc}}$  is the incipient particle after the dimerization process of the PAH and before the growth process. Figure 11 shows a comparison between the experimental soot yield measured at 1152.0 nm, where only soot particles were considered to absorb, with the computed soot yield at 0.5 ms reaction time. The compu-

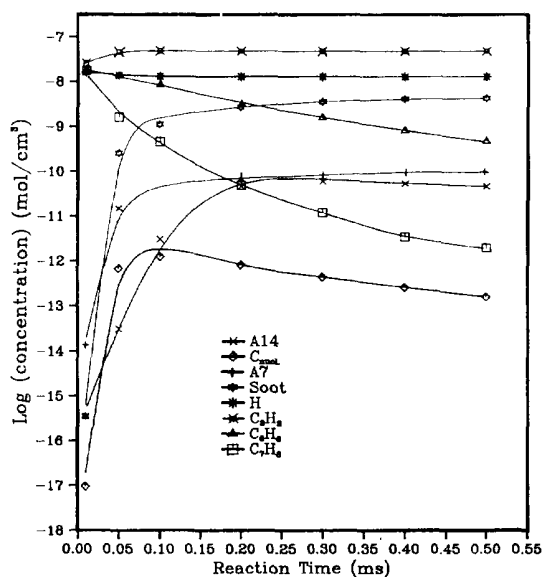


Fig. 10. Computed species concentrations as function of reaction time for 1.0% toluene at 2000 K.

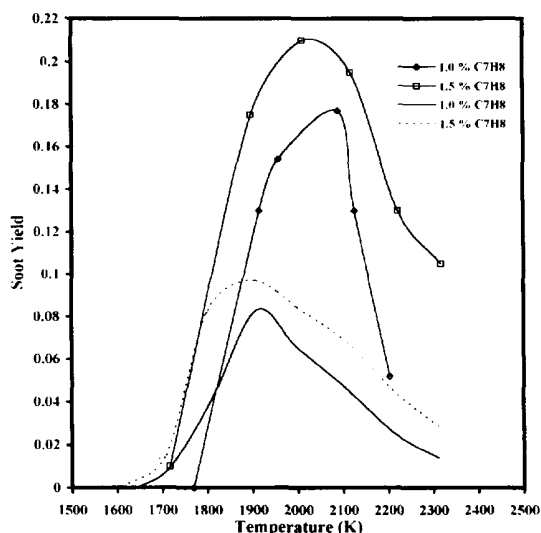


Fig. 11. A comparison between experimental results at a wavelength of 1152.0 nm (symbols) and computed soot yield for 1.0% and 1.5%, toluene pyrolysis at 0.5 ms reaction time.

tational results reproduced the experimental trends in terms of shape of the soot yield. The lack of exact quantitative agreement could be due either to the value of the complex refractive index used in the interpretation of the experimental signal, or to the insufficient knowledge of kinetic and thermochemical data, as discussed by others [10, 20].

**Alcohol Addition.** The major differences between alcohols and hydrocarbons are the presence of an oxygen atom and the reduced  $\alpha$ -C-H bond strength of the alcohols [30]. However, the longer the chain of the alcohol molecule the smaller the effect of the OH group, and therefore, the greater the hydrocarbon character of the alcohol molecule. The decomposition of methanol and ethanol at high temperature is considered to involve reactions R12–R16 [30] and these reactions yield oxygenated species capable of modifying the pyrolytic behavior of toluene. During methanol pyrolysis hydrogen atoms and molecular hydrogen are formed finally forming both carbon monoxide and molecular hydrogen. It is known that the concentration of the hydrogen atoms are very important in soot formation since they reactivate and propagate the PAH ring growth

process and thus soot (reactions i–iii), and that the overshoot of hydrogen atoms beyond their equilibrium concentration accelerates the reactivation step [5, 10, 20]. The molecular hydrogen production, during methanol decomposition, decreases the degree of the hydrogen atoms superequilibrium,  $f$ , in Eq. 15 and thus suppresses the soot formation.

$$f = \frac{[H]^2/[H_2]}{([H]^2/[H_2])_{eq}} \quad (15)$$

This is seen to be the case by comparing Fig. 10, for 1 mol.% toluene, and Fig. 12, for toluene 1 mol.% plus 2 mol.% methanol, where it can be seen that the hydrogen atom concentration is higher in the former. Secondly of course the oxidizing species are formed, such as OH and  $O_2$  (cf. Fig. 12), which preferentially produce CO rather than the soot precursors and thus soot.

Although ethanol decomposition is very similar to methanol decomposition, it produces  $C_2H_4$  (R16, R19, R20) which is a major source for ethyne formation via reactions R21–R24 and which could have a synergistic effect on soot formation as was observed experimentally (cf. Fig. 8). This arises because the production

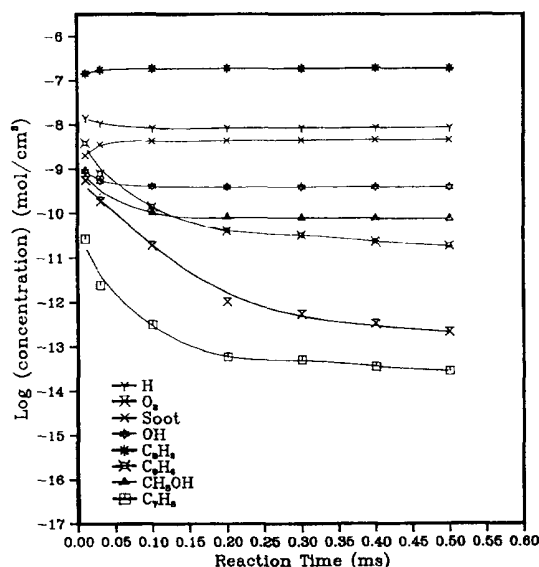


Fig. 12. Computed species concentrations as function of reaction time for the mixture of 1.0% toluene + 2.0% methanol at 2020 K.

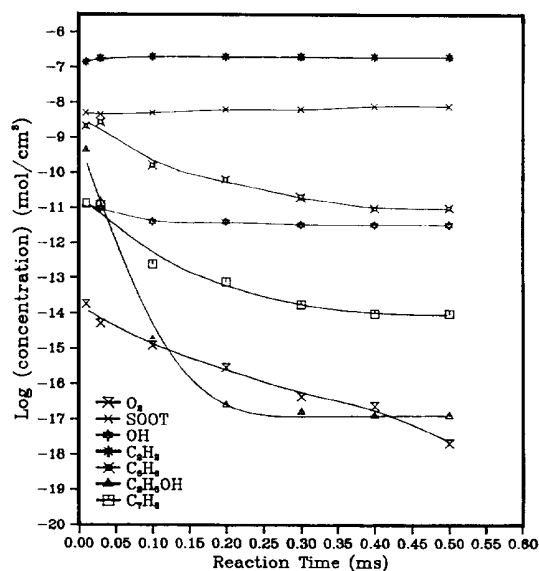


Fig. 13. Computed species concentrations as function of reaction time for the mixture of 1.0% toluene + 2.0% ethanol at 2020 K.

of  $C_2H_4$  during ethanol decomposition offsets oxidation by OH radicals as well as any reduction of the value ' $f$ ' (Eq. 15) through the formation of  $C_2H_2$ . The model thus predicted higher conversion to ethyne during ethanol decomposition as well as higher conversion of the methanol to oxidative species, such as  $O_2$  and OH, compared to ethanol decomposition as shown in Figs. 12 and 13 where selected major species concentrations for 1.0 mol.%  $C_7H_8$ /2.0 mol.%  $CH_3OH$  and 1.0 mol.%  $C_7H_8$ /2.0 mol.%  $C_2H_5OH$  at 2020 K are shown, respectively. The higher conversion to oxidizing species resulted in a greater reduction of the soot yield by  $CH_3OH$  addition as determined experimentally, and as shown in Fig. 14. Here the experimental soot yield at 1152.0 nm (solid lines with symbols) is shown for a mixture of 1.0 mol.%  $C_7H_8$ /2.0 mol.%  $C_2H_5OH$ . The shift of the observed experimental soot yield to higher temperatures was due to the absence of any interference by the soot precursors (PAH) which occurs when the 632.8 nm wavelength is used.

Franklach et al. [5] explained their results based on reaction R16 as the main decomposi-

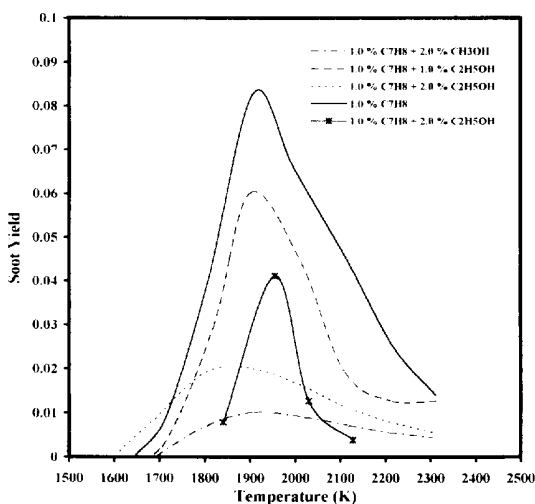


Fig. 14. A comparison between experimental at 1152.0 nm (solid line with symbols) and computed soot yield obtained during pyrolysis of toluene/ethanol and toluene/methanol mixtures at 0.5 ms reaction time.

tion reaction of ethanol and on further reaction of  $H_2O$  with H producing OH and  $H_2$ . However, reaction R16 is only 1/10 as fast as the dominant initiation step R14 [31]; thus it can not fully explain the stronger soot suppression by ethanol as observed in this way.

*Addition of Molecular Oxygen to Toluene Pyrolysis.* The oxidation model used was based on the mechanism described by Brezinsky [32]. In this mechanism, toluene is first converted to oxygenated  $C_7$  and  $C_6$  species. Next, benzene and phenyl are formed which are converted to oxygenated  $C_6$  species which later break down through loss of CO to  $C_5$  species. The oxidative process is followed by conversion of the  $C_5$  to  $C_4$  and eventually forming  $C_2$  species which in turn are oxidised to CO and  $CO_2$ . Some of these reactions are given in Table 2. Figure 15 shows the concentration of some selected species for a 1.0 mol.%  $C_7H_8$ /0.5 mol.%  $O_2$  mixture at 1803 K, while Fig. 16 shows the computed soot yield. Unfortunately a prediction of the shift of the soot yield to lower temperatures was not observed. This was due presumably to the lack of appropriate reaction pathways, being used in the model, for the

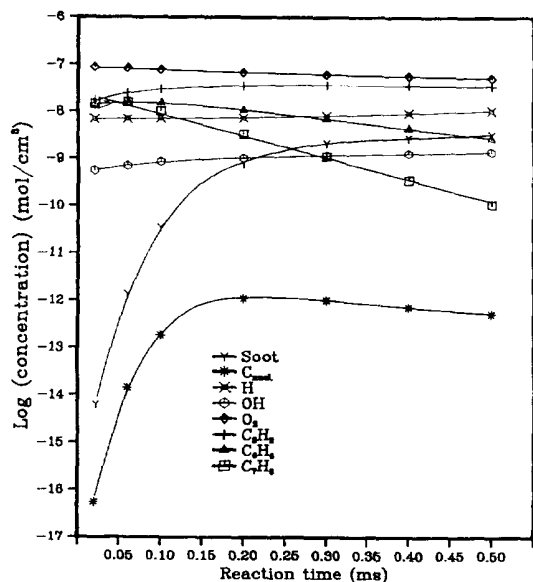


Fig. 15. Computed species concentrations as function of reaction time for the mixture of 1.0% toluene + 0.5% oxygen at 1803 K.

initial oxidation of  $C_7H_7$  and its subsequent reactions. The experimental shift of the soot yield to lower temperatures was also found by Frenklach et al. [17] who suggested that the shift of the soot bell to lower temperatures during toluene oxidation could be due to the

rapid formation of  $C_6H_6$ ,  $C_4H_4$ , and  $C_2H_2$ , at lower temperatures caused by the initial attack of the molecular oxygen on toluene, which of course alters the ease of soot formation. This is possible because the chain reaction of  $O_2$  with H atoms, producing O and OH, is more important at higher temperatures and lower pressures, allowing oxidation by OH and O to occur. Also, an increase of the H atom concentration will also contribute to the shift of the bell shape to lower temperatures, since such an increase not only increases the rate of combustion but increases the rate of PAH formation (Eq. i-iii) and thus of soot [10]. An explanation for the possible H atom formation was given by Hippler et al. [33] who suggested that  $C_7H_7$  radicals are not oxidised by direct attack of  $O_2$  but through H atom formation at temperatures below 1500 K. Hence,  $C_{14}H_{14}$  formation (by  $C_7H_7$  combination) and dissociation forming  $C_{14}H_{13}$  and H atoms could explain the shift of the experimental soot yield to lower temperatures. However, in the current work this reaction step was omitted mainly due to the uncertainties governing the  $C_{14}H_{13}$  decomposition and/or oxidation pathways.

## CONCLUSIONS

The present studies led to the following conclusions:

1. Soot induction times and the rates of soot formation were measured by laser beam attenuation for toluene pyrolysis and oxidation and for pyrolysis of toluene-methanol and toluene-ethanol mixtures. Arrhenius dependences were obtained in all cases.
2. Soot yields and soot amounts were also measured. Although soot yields and soot amounts were a function of experimental variables, those measured for toluene pyrolysis and oxidation were found to be in good agreement with previously reported data.
3. The addition of methanol and ethanol to toluene suppressed soot yields from those found for toluene alone, with more pronounced results for the methanol addition. Soot suppression by methanol was as a result of oxidation by oxygenated radicals as

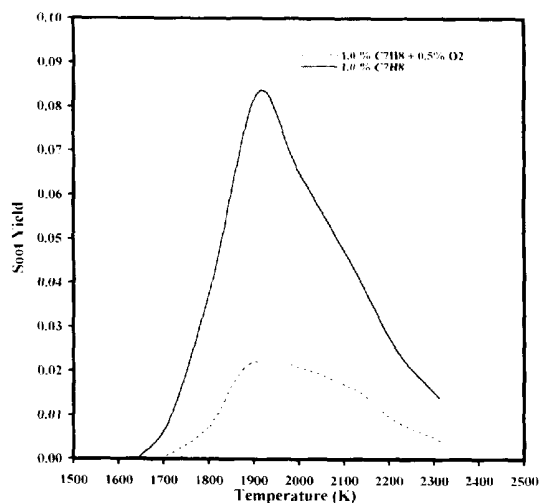


Fig. 16. A comparison of computed soot yield between pyrolysis and oxidation of toluene.

well as reduced hydrogen atom concentration. The suppression of the soot yield by ethanol not only required a concentration of 66 mol.%, for it to be significant, but initially resulted in an increase of the soot amount indicating a synergistic effect. This synergistic effect is due to the production of ethyne formed during ethanol decomposition which could offset the role of the oxidising agents. The more effective suppression of the soot yield by methanol was due to higher concentrations of oxidising species such as  $O_2$  and OH. This also arises from the fact that, when methanol is added only one carbon atom is added per oxygen atom, but with ethanol two carbon atoms are added per added oxygen atom.

4. Toluene oxidation resulted in strong soot suppression, with a shift of the bell shape of the soot yield to lower temperatures due to an alteration in the soot formation process. This last effect indicated that at lower temperatures  $O_2$  has a critical role as oxidiser rather than OH or O radicals which are only formed at rather higher temperatures.
5. The computational results reasonably reflected the experimental trends. However, the lack of precise thermochemical data as well as the insufficient knowledge of reaction rates and incomplete pathways describing the oxidation of benzyl radical and higher PAH species resulted in poor quantitative agreement of the soot yield.

## REFERENCES

1. Frenklach, M., Clary, D. W., Yuan, T., Gardiner, W. C. Jr., and Stein S. E., *Combust. Sci. Technol.* 50:79 (1986).
2. Millikan, R. C., *J. Phys. Chem.* 66:794–799 (1962).
3. Markatou, P., Wang, H., and Frenklach, M., *Combust. Flame* 93:467–482 (1993).
4. Glassman, I., *Combustion*, 2nd ed., Academic, Orlando, Florida, 1987, p. 366.
5. Frenklach, M., and Yuan, J., *Sixteenth Symposium (International) on Shock Tubes and Waves*, 1987, p. 487.
6. Alexiou, A., and Williams, A., *Amer. Chem. Soc., Div. Fuel Chem. Preprints* 36, 1547, 1991.
7. Coats, C. M., and Williams, A., *Seventeenth Symposium (International) on Combustion*, The Combustion Institute, Pittsburgh, 1979, p. 611.
8. Gardiner, W. C. Jr., Walker, B. F., and Wakefield, C. B., *Shock Waves in Chemistry*, (A. Lifshitz, Ed.), Marcel Dekker, New York, 1981, chap. 7.
9. Graham, S. C., Homer, J. B., and Rosenfeld, J. L. J., *Proc. R. Soc.* 344:259–285 (1975).
10. Frenklach, M., Yuan, T., and Ramachandra, M. K., *Energ. Fuels* 2:462–480 (1988).
11. Harris, S. J., and Weiner, A. M., *Combust. Sci. Technol.* 32:267, (1983).
12. Charalampopoulos, T. T., and Chang, H., *Combust. Sci. Technol.* 59:401, (1988).
13. Chang, H., and Charalampopoulos, T. T., *Proc. R. Soc.* 430:591 (1990).
14. Harris, S. J., Weiner, A. M., and Ashcraft, C. C., *Combust. Flame* 64:65–81 (1986).
15. Dalzell, W. H., and Sarofim, A. F., *J. Heat Transf. Trans. ASTM* 91:100–104 (1969).
16. Lee, S. C., and Tien, C. L., *Eighteenth Symposium (International) on Combustion*, The Combustion Institute, Pittsburgh, 1981, p. 1159.
17. Frenklach, M., Ramachandra, M. K., and Matula, R. A., *Twentieth Symposium (International) on Combustion*, The Combustion Institute, Pittsburgh, 1984, p. 871.
18. Wang, T. S., Matula, R. A., and Farmer, R. C., *Eighteenth Symposium (International) on Combustion*, The Combustion Institute, Pittsburgh, 1981, p. 1149.
19. Frenklach, M., Taki, S., and Matula, R. A., *Combust. Flame* 49:275–282 (1983).
20. Frenklach, M., and Wang, H., *Twenty-Third Symposium (International) on Combustion*, The Combustion Institute, Pittsburgh, 1990, p. 1559.
21. Miller, J. A., and Melius, C. F. *Combust. Flame* 91:21–39 (1992).
22. Miller, J. A., *Twenty-Third Symposium (International) on Combustion*, The Combustion Institute, Pittsburgh, 1990, p. 91.
23. McKinnon, J. T., and Howard, J. B., *Twenty-Fourth Symposium (International) on Combustion*, The Combustion Institute, Pittsburgh, 1992, p. 965.
24. Leung, K. M., Lindstedt, R. P., and Jones, W. P., *Combust. Flame* 87:289–305 (1991).
25. Pamidimukkala, K. M., Kern, R. D., Patel, M. R., Wei, H. C., and Kiefer, J. H., *J. Phys. Chem.* 91:2148–2154 (1987).
26. Rao, V. S., and Skinner, G. B., *J. Phys. Chem.* 93:1864–1869 (1989).
27. Brouwer, L. D., Muller-Markgraf, W., and Troe, J., *Twentieth Symposium (International) on Combustion*, The Combustion Institute, Pittsburgh, 1984, p. 799.
28. Muller-Markgraf, W., and Troe, J., *J. Phys. Chem.* 92:4899–4905 (1988).
29. Braun-Unkhoff, M., Frank, P., and Just, Th., *Twenty-Second Symposium (International) on Combustion*, The Combustion Institute, Pittsburgh, 1989, p. 1053.
30. Norton, T. S., Ph.D. thesis, The University of Princeton, 1989.
31. Tsang, W., *Int. J. Chem. Kinet.* 8:193–203 (1976).
32. Brezinsky, K., *Prog. Energ. Combust. Sci.* 12:1–24 (1991).
33. Hippler, H., Reihs, C., and Troe, J., *Twenty-Third Symposium (International) on Combustion*, The Combustion Institute, Pittsburgh, 1990, p. 37.

34. Tanzawa, T., and Gardiner, W. C. Jr., *J. Phys. Chem.* 84:236–239 (1980).
35. Warnatz, J., *Combustion Chemistry*, Chapter 5, Springer-Verlag, New York, (1984).
36. Westmoreland, P. R., Dean, A. M., Howard, J. B., and Longwell, J. P., *J. Phys. Chem.* 93:8171–8180 (1989).
37. Wu, C. H. and Kern, R. D., *J. Phys. Chem.* 91:6291–6296 (1987).
38. McLain, A. G., Jaschimowski, C. J., and Wilson, C. H., NASA Technical Paper, 1472 (1979).
39. Brezinsky, K., Litzinger, T. A., and Glassman, I., *Int. J. Chem. Kinet.* 16:1053–1074 (1984).
40. Solly, R. K., and Benson, S. W., *J. Am. Chem. Soc.* 93:2127–2131 (1971).
41. Mardonich, S., and Felder, W., *J. Phys. Chem.* 89:3556–3561 (1985).
42. Fujii, N., and Asaba, T., *Fourteenth Symposium (International) of Combustion*, The Combustion Institute, Pittsburgh, 1973, p. 433.
43. Bittker, D. A., *Combust. Sci. Technol.* 79:49 (1991).
44. Pitz, W. J., Westbrook, C. K., Proscia, W. M., and Dryer, F. L., *Twentieth Symposium (International) on Combustion*, The Combustion Institute, Pittsburgh, 1984, p. 831.

Received 3 February 1994; revised 12 December 1994